

Self-powered nanowire devices

Sheng Xu[†], Yong Qin[†], Chen Xu[†], Yaguang Wei, Rusen Yang and Zhong Lin Wang^{*}

The harvesting of mechanical energy from ambient sources could power electrical devices without the need for batteries. However, although the efficiency and durability of harvesting materials such as piezoelectric nanowires have steadily improved, the voltage and power produced by a single nanowire are insufficient for real devices. The integration of large numbers of nanowire energy harvesters into a single power source is therefore necessary, requiring alignment of the nanowires as well as synchronization of their charging and discharging processes. Here, we demonstrate the vertical and lateral integration of ZnO nanowires into arrays that are capable of producing sufficient power to operate real devices. A lateral integration of 700 rows of ZnO nanowires produces a peak voltage of 1.26 V at a low strain of 0.19%, which is potentially sufficient to recharge an AA battery. In a separate device, a vertical integration of three layers of ZnO nanowire arrays produces a peak power density of 2.7 mW cm⁻³. We use the vertically integrated nanogenerator to power a nanowire pH sensor and a nanowire UV sensor, thus demonstrating a self-powered system composed entirely of nanowires.

Harvesting energy directly from the environment is one of the most effective and promising approaches for powering nanodevices^{1–4}. Mechanical energy surrounds us in our daily life, taking the form of sonic waves, mechanical vibrations and impacts, air flow, friction, hydraulic and ocean waves, all available around the clock. ZnO nanowires are unique in their suitability not only for the fabrication of nanosensors^{5–8}, but also for scavenging mechanical energy^{1,9,10}. One creative initiative is to use ZnO nanowires, alone, to build an integrated nanopower–nanodevice system that is self-driven, with no battery or external power source. The most challenging task in achieving this aim is probably the creation of an energy-scavenging unit that works over a range of frequencies. In previous work, a d.c. piezoelectric nanogenerator based on vertically aligned ZnO nanowire arrays has been demonstrated, which relies on a zig-zag top electrode. This acts like an array of atomic force microscopy (AFM) tips that force the nanowires to bend in response to the external mechanical agitation caused by an ultrasonic wave⁹. The contact between the top electrode and the nanowires switches instantaneously on and off for each cycle of the driving action, and a relative scrubbing and sliding between the two may result in wearing and increased contact resistance/instability^{11,12}. Here, we report innovative and much improved steps towards achieving a high-power-output, a.c. nanogenerator based on vertically or laterally aligned ZnO nanowire arrays in which there are solid bonds/contacts between the electrodes and the ends of the nanowires. A periodic, low-frequency, uniaxial strain is applied to the ZnO nanowires by an external mechanical action to create a piezoelectric potential along the nanowires, which results in an alternating electrical output. A three-layer integration of the vertical nanowire array integrated nanogenerator (VING) enhances the output voltage up to 0.243 V. In addition, a multiple lateral-nanowire-array integrated nanogenerator (LING) has also been fabricated by combining a rational chemical growth with novel nanofabrication. A maximum voltage output of 1.26 V has been generated by integrating 700 rows of lateral ZnO nanowire arrays. Finally, the integration of a VING with a ZnO nanowire-based pH or UV nanosensor has allowed the demonstration of a ‘self-powered’ nanosystem that is built solely from ZnO nanowires. This is a key step towards developing an independent, reliable and sustainable unit for use in environments in which a dynamic

compressive stress/strain is available, such as in shoe pads, vehicle tyres, under carpets or floors and even in ocean waves.

Three-dimensionally integrated VING

The key to a self-powered nanosystem is the fabrication of a nanogenerator that provides high output voltage and power. The fabrication stages for a VING are illustrated in Fig. 1. Vertical ZnO nanowires (Fig. 1g) were rationally grown on a gold-coated flat surface using a wet chemical method at a temperature below 100 °C (ref. 13). The figures of merit for using ZnO nanowires for energy harvesting are presented in the Supplementary Information. A layer of polymethyl-methacrylate (PMMA) was spin-coated onto the nanowires to fully wrap them from top to bottom (Fig. 1c,h), largely improving the stability and mechanical robustness of the entire structure, and also preventing possible short-circuiting between the substrate and the top electrode. Oxygen plasma etching was performed, leaving behind fresh and clean tips on the nanowires (Fig. 1i, inset). A piece of silicon wafer coated with a 300-nm-thick platinum film was then placed in direct contact with the nanowires (Fig. 1e), creating a Schottky contact at the interface. Measurement was carried out in a Faraday cage, using a linear motor stimulator to generate the mechanical strain at an impact speed of 0.1 m s⁻¹. Typical *I*–*V* characteristics of the VING are shown in Supplementary Fig. S1, with a rectification ratio of ~1,000 at a bias voltage of ±0.4 V.

The working principle of the VING lies in the coupling of piezoelectric and semiconducting properties. In the existing literature it is shown that wurtzite structured nanowires grow uniaxially parallel to the *c* axis^{14–17}. The crystallographic alignment of the nanowires indicates their piezoelectric alignment in response to the external stress. When a nanowire is under uniaxial strain, a separation of the static ionic charge centres in the tetrahedrally coordinated Zn–O units results in a piezoelectric potential gradient along the *c* axis of the nanowire (Fig. 1f). Because the *c*-axes of the nanowires are aligned parallel to one another, the piezoelectric potentials created along each nanowire have the same tendency of distribution, leading to an enhanced macroscopic behaviour. When a stress is applied, the nanowires are under uniaxial compression, with a negative piezoelectric potential at the tip Schottky contact side, for example, and a positive piezoelectric potential at the bottom

School of Materials Science and Engineering, Georgia Institute of Technology, Atlanta, Georgia 30332-0245, USA; [†]These authors contributed equally to this work. *e-mail: zlwang@gatech.edu

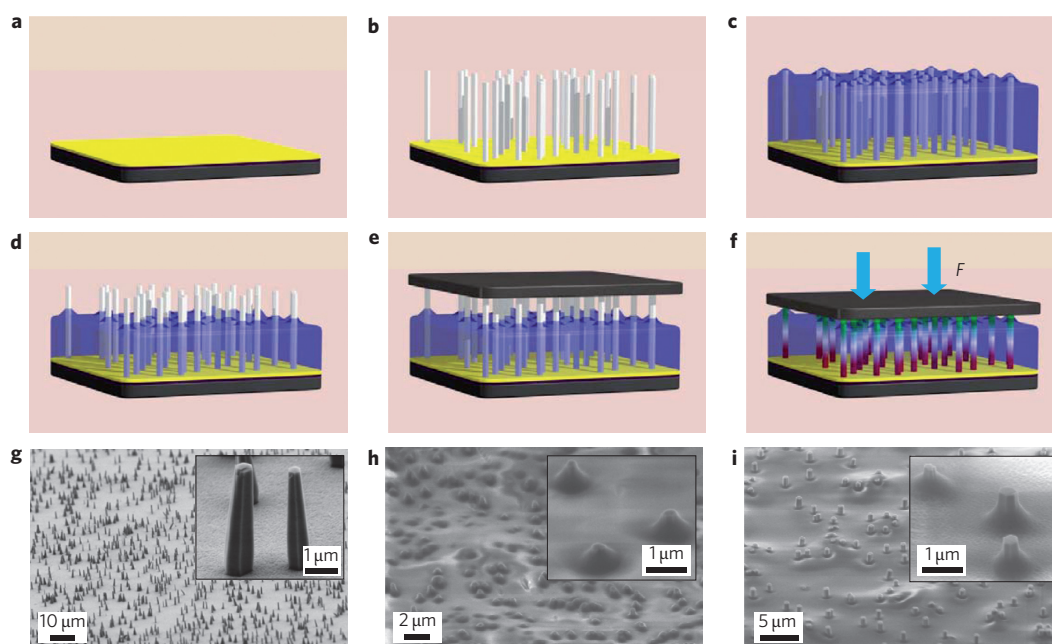


Figure 1 | Steps for fabrication of VING. **a–f**, On a gold-coated silicon wafer (**a**), ZnO nanowire arrays (**b**) are grown by low-temperature hydrothermal decomposition. PMMA, applied by spin coating (**c**), covers both the bottom and tips of the nanowire arrays. After oxygen plasma etching (**d**), the tips of the nanowires are exposed, fresh and clean, but the main body and bottoms of the nanowires are still fully enclosed, greatly improving the robustness of the structure. A platinum-coated flat electrode is placed on top of the nanowires (**e**) to form a firm Schottky contact. When a uniaxial stress is applied at the top electrode (**f**), the nanowires are readily compressed, the straining of the crystallographically aligned nanowires generating a macroscopic piezoelectric potential along the *c*-axis growing direction of the nanowires. **g–i**, SEM images of the as-grown ZnO nanowire arrays on the substrate (**g**), after spin-coating with PMMA (**h**) and after oxygen plasma etching (**i**).

ohmic contact side (see Supplementary Information). The negative piezoelectric potential rises up the conduction band and the Fermi level at the tip relative to the bottom electrode¹⁸. Electrons will therefore flow from the tip to the bottom through the external circuit. The Schottky barrier at the tip, however, obstructs the electrons from passing through the interface. These electrons are therefore blocked and accumulate around the bottom of the nanowires, consequently elevating the Fermi level at the bottom until the piezoelectric potential is fully ‘screened’ and the Fermi levels of each side reach a new equilibrium. During this process, the flow of electrons via the external circuit is detected as an electric pulse. As the external force is removed and the compressive strain is released, the piezoelectric potential inside the nanowires diminishes. The electrons accumulated at the bottom then undoubtedly flow back via the external circuit (if leakage is negligible), creating an electric pulse in the opposite direction. The role of the Schottky barrier is to prevent those mobile charges from passing through the nanowire–metal contact interface. The piezoelectric potential acts as a ‘charging pump’ that drives the electrons to flow. By the same token, the same process occurs if the Schottky barrier is at the bottom or both sides of the nanowires.

The presence of a Schottky contact at least at one end of the nanowires is essential for the operation of the VING, as demonstrated in the following control experiments. First, a VING with ohmic contacts at both ends gave no output signal (Supplementary Fig. S2, pink lines). Second, to exclude the effect of a change in capacitance in the mechanical pressing and releasing processes (which could potentially introduce output signals due to an effect from the measurement system), no oxygen plasma etching was performed, and the ZnO nanowires were insulated from the top platinum electrode by the PMMA film. The electric signal generated by such a device was too small to be detected (Supplementary Fig. S2, green lines). Third, measurements were carried out to exclude electromagnetic interference. We allowed

the mechanical arm of the linear motor stimulator to vibrate back and forth to a distance very close to the top surface of the packaged VING, but without making direct physical contact. The output could not be distinguished from the noise (Supplementary Fig. S2, purple lines). Finally, polarity reversion tests and linear superposition tests further showed that the signals were truly from the VING^{13,19,20} (Supplementary Fig. S3).

The output voltage and current could be greatly enhanced by linearly integrating a number of VINGs. Three VINGs with individual output voltages of 80, 90 and 96 mV, respectively, were connected in serial, leading to an output voltage of 0.243 V (Fig. 2a). Likewise, three VINGs with individual output current densities of 6.0, 3.9 and 8.9 nA cm⁻², respectively, were connected in parallel, leading to an output current density of 18.0 nA cm⁻² (Fig. 2b). The maximum power density of the VING can be estimated using the peak values of the output voltage and current. By conservatively assuming that one-third of all the nanowires were actively generating electricity in a perfectly synchronized process, the power density was estimated to be 2.7 mW cm⁻³, which is 6 to 11 times that generated by a PZT cantilever^{21,22}.

Theoretical calculations have shown that, within the elastic linear mechanics regime, the output voltage of a single nanowire is linearly proportional to the magnitude of its deformation²³. The ZnO nanowires in the VING were all connected in parallel between the two electrodes. Undoubtedly, as we increase the pressing force acting on the nanowires, their deformation becomes larger, and the output voltage will linearly scale up (Fig. 2c). It must be noted that a large fraction of the applied stress was consumed in overcoming the elasticity of the packaging material (1–2 mm in thickness) around the VING. The magnitude of the output voltage also depended on the straining rate at which the stress was applied (Supplementary Fig. S4). The output signals of the VING were stable over a long period of time (Supplementary Fig. S5).

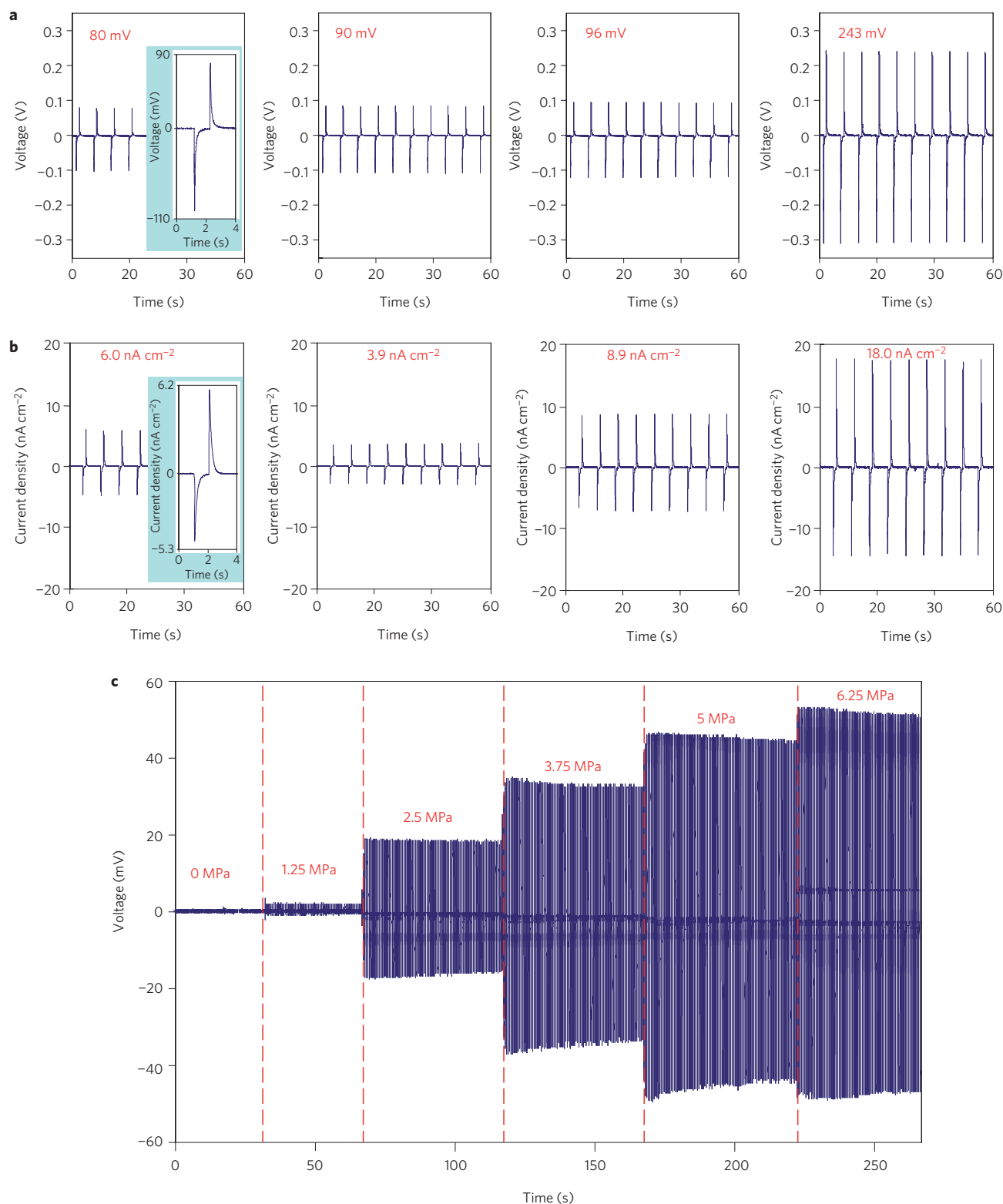


Figure 2 | Linear superposition and output voltage versus stress characteristics of VING. **a**, Enhancing the output voltage of the VINGs by integrating them in serial. Individual VING devices produce output voltages of 80, 90 and 96 mV, respectively. When the three VINGs are connected in series, the voltage increases to 243 mV. **b**, Linear superposition of output current when the VINGs are connected in parallel. Individual VING devices produce output current densities of 6.0, 3.9 and 8.9 nA cm⁻², respectively. When the three VINGs are connected in parallel, the output current density increases to 18.0 nA cm⁻². Insets in the left panels of **a** and **b** are enlarged views of a single pulse. **c**, Magnitude of the output voltage as a function of the magnitude of the compressive stress at a frequency of 2 Hz. The VING is built using ZnO nanowires with a tip diameter of ~ 300 nm and length of 4 μm . The size of the VING was ~ 4 mm². The total number of nanowires grown in the nanogenerator was $\sim 75,000$ (area density, 1.9×10^6 cm⁻²). As the applied stress is gradually increased from 0 to 1.25, 2.5, 3.75, 5 then 6.25 MPa, the output voltage increases almost linearly. The impact speed of the mechanical trigger was 0.1 m s⁻¹, but it was hard to correlate this to the straining rate in the nanowires because the damping effect of the packaging material around the nanogenerator was difficult to quantify.

High-output flexible LING

A single nanowire-based nanogenerator on a flexible substrate can be driven by the mechanical agitation present in our living environment¹⁸, including that resulting from human or animal motion^{24,25}. It is essential to enhance the output power by integrating contributions from multiple nanowires (Fig. 3a). Because the diameter of a nanowire is much smaller than the thickness of the substrate film, all the nanowires on a substrate are subjected to a pure tensile strain when the substrate is stretched. Each active nanowire works as a 'charging pump', and is independent of the other nanowires as the substrate is bent and released¹⁸. If the charging and discharging processes of many nanowires could be synchronized, the output a.c. voltages could be added constructively (Fig. 3a), resulting in a high output voltage.

Several factors have to be considered when integrating the outputs of many nanowires. First, there should be a Schottky contact at least at one side of the nanowires¹⁸ (Fig. 3b). Second, the contacts at the two ends should be robust enough that the mechanical deformation can be effectively transmitted from the electrodes to the nanowires. Third, all the nanowires should have the same crystallographic orientation to ensure that the polarities of the generated piezoelectric potentials are aligned. The nanowires therefore need to be rationally grown, directly on the substrate, rather than by chemical assembly (which usually gives orientational alignment but not crystallographic polarity alignment). Finally, all of the nanowires must be stretched and released in a synchronized manner, so that the piezoelectric potentials generated by all of them are in the same direction and occur at the same time (Fig. 3c), resulting in an enhanced output voltage.

The experimental procedures in Fig. 4 were designed to fabricate the LING to meet all of the above requirements. The first step was to grow crystallographically aligned nanowires parallel to the substrate using a chemical approach at below 100 °C (Fig. 4a,b)²⁶. A thick layer of gold was then deposited using an aligned mask technique to connect the tips of the nanowires with the gold electrode (Fig. 4c,d) so that the nanowires were robust to mechanical deformation without there being any loose contacts (Fig. 4e,f).

A periodic external force was used to deform the flexible substrate so that the nanowires experienced a cyclic stretching–releasing deformation process. A push to the middle of the substrate by the linear motor resulted in a tensile strain across all the rows of the nanowires constructed on top of the substrate (Fig. 4g; Supplementary Fig. S6), creating a macroscopic piezoelectric potential resulting from the crystallographic alignment of the nanowires. In the present experiments, the flexible substrate was pushed with a relatively fast straining rate and held in position for 1 s before being released. An interval of 2 s was left before pushing again.

Integrating more ZnO nanowires, improving the interconnection of the electrodes and nanowires, and increasing the strain or straining rate are all important targets for enhancing the output voltage and current of the LING. Figure 5 shows the output voltage and current of a LING composed of 700 rows of nanowires, with each row containing ~20,000 nanowires. When the substrate was mechanically deformed, the LING demonstrated an average output voltage of ~1.2 V and a current pulse of ~26 nA (Fig. 5a,b) at a straining rate of 2.13% s⁻¹ and strain of 0.19%. Note that the magnitudes of the voltage and current peaks of the LING were slightly different in the stretching and releasing stages because of the different straining rates of the two processes. A maximum voltage of 1.26 V and maximum current of 28.8 nA were demonstrated (Fig. 5a,b). By assuming that one-third of the nanowires were actively contributing to the current output, the average current generated by one nanowire can be estimated to be 4.3 pA, which is compatible with the ~10 pA obtained when a

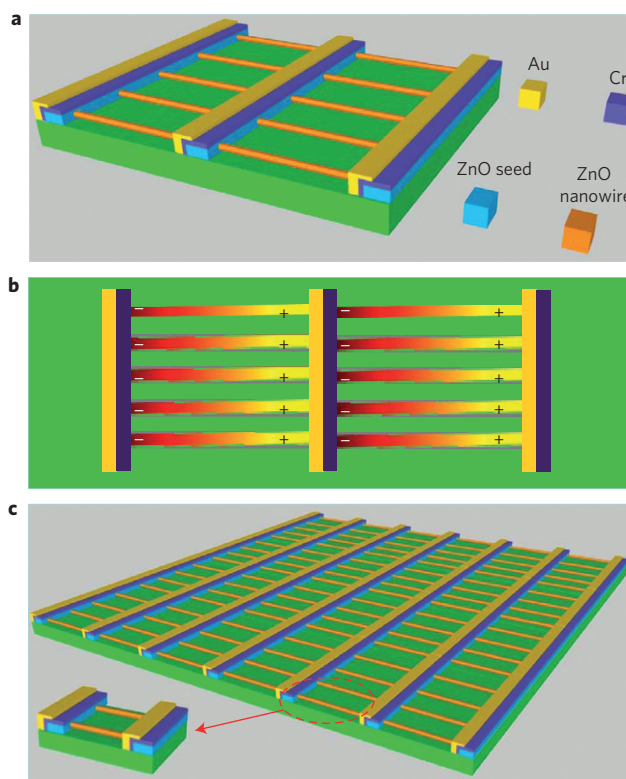


Figure 3 | Design of LING array. **a**, Schematics of LING structure, in which gold and chromium are used to create Schottky and ohmic contacts at the two ends of the lateral nanowires, respectively. **b**, Working mechanism of the LING when subjected to a mechanical deformation, where the '+/-' signs indicate the polarity of the local piezoelectric potential created in the nanowires. **c**, Schematics of a LING array comprising many rows of lateral nanowires.

nanowire is triggered by an AFM tip²⁷. If we exclude the area occupied by the electrodes, a peak output power density of ~70 nW cm⁻² has been obtained.

Like the VING, increasing the strain is an effective way to achieve a high output voltage and current²³. Supplementary Fig. S7a shows the output current and voltage from a LING of 100 rows of nanowires measured at different strains. Both the output current and voltage increased monotonously with increasing strain. Increasing the straining rate is also effective in raising the output voltage. Shown in Supplementary Fig. S7b is a measurement from a LING as a function of the straining rate by fixing the maximum strain. Clearly, both the output voltage and current increase with an increase in the straining rate.

The output voltage has been greatly enhanced by lateral integration, but the output current is rather limited, which is probably attributable to the following factors. First, the orientational alignment of the as-grown lateral nanowires was not perfect and only a fraction of them were in contact with the gold electrode (Fig. 4b). Among the nanowires that were in contact, only a fraction of them were actually actively outputting electricity, and the inactive nanowires acted as a capacitance to reduce the output current and voltage¹¹. Second, the bonding between the gold and ZnO was not very solid, and could become loose during repeated mechanical stretching cycles. We only applied a maximum strain of 0.19% in our experiments, which is much smaller than the 6% maximum tensile strain predicted theoretically for a ZnO nanowire before fracture²⁸. Finally, the inner resistance of the entire integrated sheet was 1–10 MΩ, which significantly reduced the total output current.

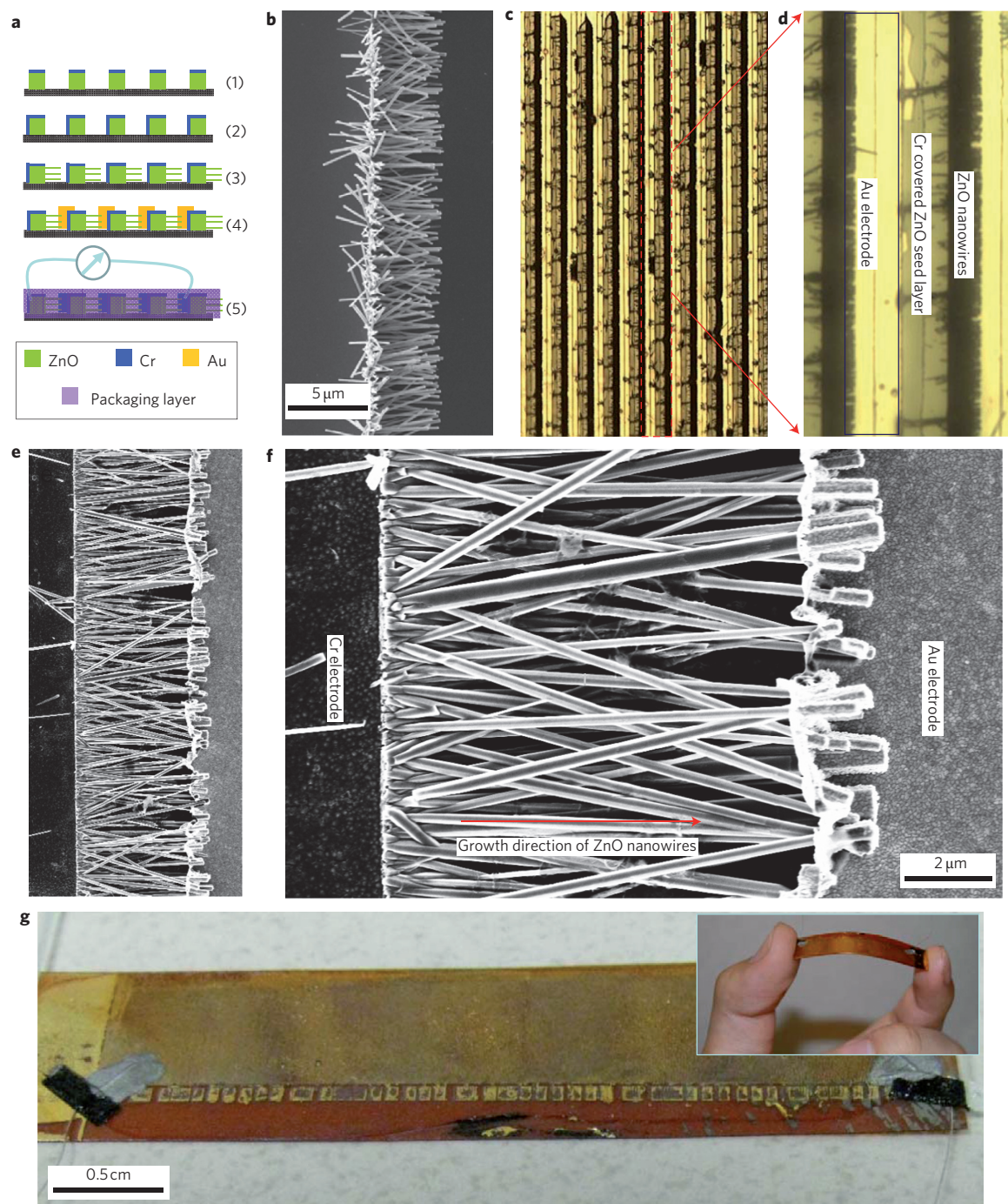


Figure 4 | Fabrication process and structural characterization of LING. **a**, Schematics for the rational growth of nanowire arrays orientationally aligned parallel to the substrate surface (see Methods for details). **b**, SEM image of a row of a laterally grown ZnO nanowire array. **c,d**, Optical microscopy images of LING structure with many rows of nanowire arrays. **e,f**, SEM images of a single-row LING structure. **g**, Low-magnification optical image of the LING. Inset: demonstration of the LING flexibility.

Towards a self-powered nanosystem

The VING was integrated with a single nanowire-based nanosensor to demonstrate a ‘self-powered’ nanosystem, the two elements being separate components that were connected in series to form a loop. As shown in the insets in Fig. 6, a VING was connected to a ZnO nanowire-based pH sensor (Fig. 6a)²⁹, or UV sensor (Fig. 6b)³⁰, and the voltage across the nanosensor was monitored by a voltmeter. The pH sensor was coated with a 10-nm layer of Si₃N₄, which was thin enough to allow electrostatic interaction between the surface adsorbed charges and the carriers in the nanowire. By powering

the pH sensor using a VING that generated an output voltage of ~40 mV, a clear sensitivity to local pH change was observed (Fig. 6a). When the buffer solution was basic, the surface of the nanosensor was dominated by $-O^-$ groups. Those negatively charged groups resulted in depletion regions at the surface of the n-type ZnO nanowire, which increased the resistance of the nanowire. The voltage drop on the nanowire was therefore relatively high. As the buffer solution changed from basic to acidic, the groups on the surface of the nanosensor gradually changed from $-O^-$ to $-OH_2^+$ groups. The depletion regions at the nanowire

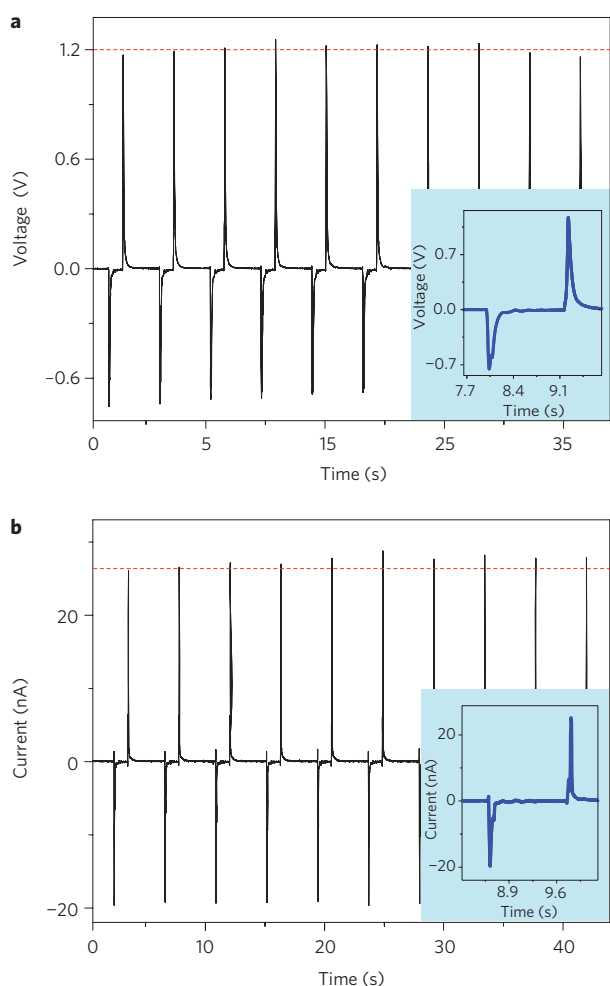


Figure 5 | Performance of LING. a,b, Open-circuit output voltage (a) and corresponding short-circuit output current (b) measured for a LING structure comprising 700 rows of nanowire arrays. The maximum output voltage peak reaches 1.26 V. The insets are output voltage and current for one cycle of the mechanical deformation. The LING is periodically deformed at a straining rate of $2.13\% \text{ s}^{-1}$ to a maximum strain of 0.19% (Supplementary Fig. S6).

surface therefore diminished, lowering its resistance. As the pH value of the testing buffer solution was lowered from 10.01, 9.18, 7.01, 6.86, and to 4.01, the voltage drop on the pH sensor changed accordingly (Fig. 6a).

A VING was also used to drive the operation of a ZnO nanowire-based UV sensor (Fig. 6b). When there was no UV light, the resistance of the UV sensor was $\sim 10 \text{ M}\Omega$ (Supplementary Fig. S8a), which was of the same order as the inner resistance of the VING (Supplementary Figs S9,S10). The corresponding voltage drop on the nanosensor was $\sim 25 \text{ mV}$, as shown in Fig. 6b. When the nanosensor was illuminated by UV light, its resistance dropped to $\sim 500 \text{ k}\Omega$ (Supplementary Fig. S8b), which is 20 times lower in magnitude than the value before illumination. The voltage drop on the nanosensor could barely be distinguished from the noise. This unambiguously indicates that a VING of 20–40 mV can power up a nanosensor. When using a variable resistor, the voltage across the resistor was found to be sensitive to the magnitude of its resistance, and the result fits well with linear circuit theory (Supplementary Figs S9,S10).

Conclusions

We have presented two approaches for using vertically and laterally aligned ZnO nanowire arrays to convert mechanical energy into

electricity using materials that are environmentally friendly and biocompatible³¹. The vertical and lateral nanowires were in full contact at both ends. Using the crystallographic alignment of the nanowires, a macroscopic piezo-potential is created when the nanowires are subjected to a uniaxial compressive or tensile strain, which drives a transient flow of electrons in the external circuit.

We integrated three VINGs in series to achieve an enhanced output voltage of 0.243 V, and then integrated them in parallel to obtain an improved output current density of 18 nA cm^{-2} . A peak output power density of 2.7 mW cm^{-3} has also been achieved. This demonstrates the great potential for layer-by-layer three-dimensional integration in applications where a dynamic compressive stress/straining is available, such as in shoe pads, vehicle tyres and under carpets or floors.

Based on a rational chemical synthesis of ZnO nanowire arrays parallel to a general flexible substrate, a LING made of 700 rows of nanowires raised the output voltage to 1.26 V in response to a low-frequency mechanical strain of 0.19% at a straining rate of $2.13\% \text{ s}^{-1}$. Fabrication was carried out at a temperature below 100°C , and thus could be applied to virtually any materials at low cost. Experimental observation has shown that ZnO nanowires are robust and fatigue-free³². Therefore, a layer-by-layer integration of LINGs is possible for fabricating three-dimensional energy harvesters that have a high enough output to power small electronic devices. Our current work demonstrates a technological route to improving the performance of nanogenerators for practical applications, with the possibility of harvesting large-scale power such as wind or ocean waves.

A solely nanowire-based, self-powered nanosensor unit has been demonstrated. The VING was directly integrated with a ZnO nanowire-based pH or UV sensor to demonstrate the feasibility of independent and sustainable operation of a nanosensor using a VING with an output voltage of 20–40 mV. Such powering of a nanosensor is a pivotal step towards building self-powered, solely nanowire-based nanosystems.

Methods

Growth of vertically aligned ZnO nanowire arrays for the VING. A piece of Si(100) wafer was cleaned by a standard cleaning process. A 20-nm layer of titanium and a 50-nm-thick layer of gold were consecutively deposited on top of the silicon wafer by magnetron plasma sputtering. The titanium thin film served as an adhesion layer to buffer the large lattice mismatch between the Si(100) surface with native oxide and Au(111) surface to improve interfacial bonding. The gold thin film was expected to act as an 'intermediate layer' to assist growth. The substrate was then annealed at 300°C for 1 h to increase the crystallinity of the gold thin film. The nutrient solution was composed of a 1:1 ratio of zinc nitrate hexahydrate and hexamethylenetetramine (HMTA). The substrate was placed face down at the top of the nutrient solution surface³³. Owing to surface tension, the substrate could float at the top of the solution surface without sinking. The solution was then heated in a mechanical convection oven to 95°C for 4 h.

Fabrication of LING. The detailed fabrication of the LING was accomplished following a five-step procedure (Fig. 4a). The seed layer was first fabricated by partially covering patterned ZnO stripes with a chromium layer. To achieve this, a Kapton[®] film with a thickness of $125 \mu\text{m}$ (Dupont) was cleaned using a standard procedure. A photoresist (Shipley Microposit 1813) was spun onto this film. The film was then patterned using a mask aligner, followed by consecutive deposition of 300-nm-thick ZnO and 5-nm-thick chromium layers. After developing and lifting off, a stripe-shaped ZnO pattern with a top layer of chromium was achieved (Fig. 4a(1)). The second step was to deposit chromium only at one side of the ZnO stripe, leaving the other side exposed. The entire structure was spin-coated with a layer of photoresist, then a mask was used to cover one side while the other side was exposed for each ZnO strip by controlling its offset position. A layer of chromium (10 nm) was sputtered. A lift-off produced the structure shown in Fig. 4a(2). The third step involved the growth of ZnO nanowire arrays (Fig. 4a(3)) using the wet chemical method at 80°C for 12 h. Figure 4b shows a typical scanning electron microscopy (SEM) image of a horizontally grown ZnO nanowire array. The length of each nanowire is $\sim 5 \mu\text{m}$ and the diameter several hundred nanometres (Fig. 4e); the length and diameter of the nanowires could be easily controlled by refreshing the growth solution and increasing the growth time to ensure they are in contact with the other electrode. In the fourth step, the gold electrode was deposited only on the side of the strip where the chromium layer was present (Fig. 4a(4)). The thickness of

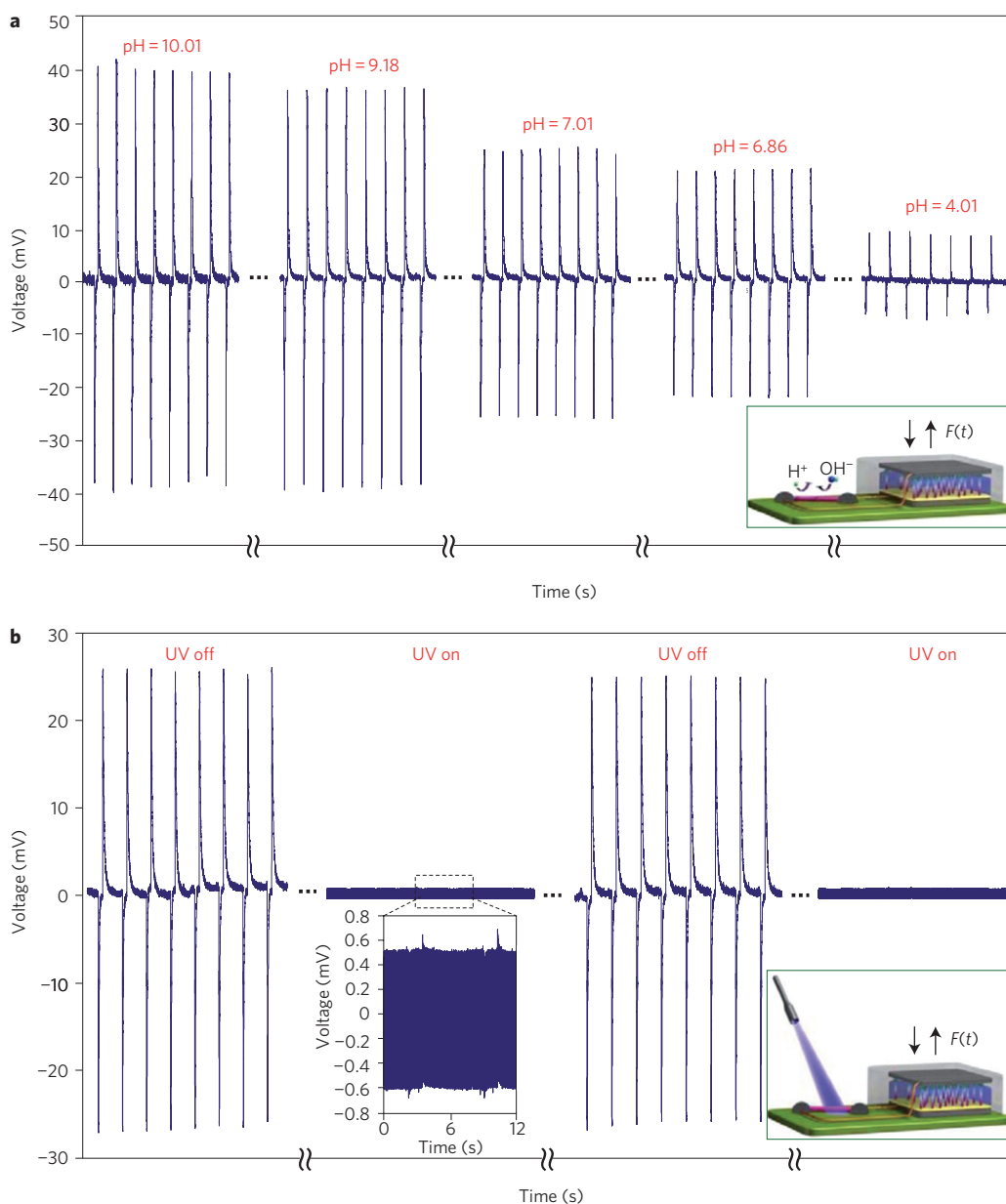


Figure 6 | Integration of a VING (4 mm² in size) with nanosensors to demonstrate the solely nanowire-based 'self-powered' nanosystem. The mechanical impacts are applied at a frequency of 0.16 Hz, and each cycle produces a pair of positive–negative output voltage/current signals. For illustration purposes, only stabilized signals are displayed on the plot after changing the buffer solution or turning the UV light on or off. **a**, Voltage drop across a single ZnO nanowire-based pH sensor powered by a VING with an output voltage of ~40 mV, showing a stepwise dropping of the voltage across the nanosensor as a function of its local pH value. The ZnO nanowire was covered with a thin layer of Si₃N₄ and the testing was carried out within 1 h so that the etching effect from the solution was negligible. **b**, Voltage drop across a ZnO nanowire-based UV sensor powered by a VING with an output voltage of ~25 mV. When the UV light is off, the resistance of the nanowire is comparable to the inner resistance of the VING, and the nanowire therefore shares a substantial amount of voltage. When the UV light is turned on, the resistance of the nanowire decreases to a level that is non-competitive to the VING, and the voltage drop across the nanowire is very small. The insets are schematics of the nanowire-based nanopower–nanodevice systems.

the gold layer was controlled to ensure a good connection between the nanowires and the electrodes (Fig. 4f). Finally, the entire structure was packaged using insulating soft polymer, such as a photoresist (Fig. 4a(5)). This packaging layer fixed the ZnO nanowires firmly onto the substrate, allowing them to be synchronized throughout the mechanical stretching or releasing stages. Figure 4c,d shows optical microscopy images of the fabricated LING. The ZnO nanowire arrays are connected with each other, head-to-tail, by patterned electrodes. Figure 4e,f shows SEM images of the as-fabricated LING structure. A fully packaged, large-sized LING is presented in Fig. 4g, and its flexibility is demonstrated in the inset.

Fabrication process for the UV and pH sensors. The ZnO nanowires used for both the UV and pH sensors were synthesized by physical vapour deposition without any catalyst³⁴. The source material was simply ZnO powder. The UV and pH sensors

were fabricated by laying a ZnO nanowire across the pre-patterned gold electrodes. The two ends of the nanowires were fixed by deposition of platinum:gallium using a focused ion beam microscope, which provided ohmic contacts at the two ends. For the pH sensor, another 10-nm-thick conformal layer of Si₃N₄ was coated on top of the ZnO nanowires by plasma enhanced chemical vapour deposition to protect the nanowires from being dissolved by the buffer solutions (HANNA Instruments), which had different pH values from the PI point (PI = 9.5) of ZnO³⁵. The response of the UV sensor was characterized by a portable UV lamp (Spectroline, Model ENF-280C, 365 nm). All of the testing was carried out in an ambient environment at room temperature.

Received 2 November 2009; accepted 17 February 2010;
published online 28 March 2010

References

- Wang, Z. L. & Song, J. H. Piezoelectric nanogenerators based on zinc oxide nanowire arrays. *Science* **312**, 242–246 (2006).
- Tian, B. Z. *et al.* Coaxial silicon nanowires as solar cells and nanoelectronic power sources. *Nature* **449**, 885–890 (2007).
- Wang, Z. L. Self-powered nanotech–nanosize machines need still tinier power plants. *Sci. Am.* **298**, 82–87 (2008).
- Pan, C. F. *et al.* Nanowire-based high performance ‘micro fuel cell’: one nanowire, one fuel cell. *Adv. Mater.* **20**, 1644–1648 (2008).
- Dorfman, A., Kumar, N. & Hahm, J. I. Highly sensitive biomolecular fluorescence detection using nanoscale ZnO platforms. *Langmuir* **22**, 4890–4895 (2006).
- Zang, J. F. *et al.* Tailoring zinc oxide nanowires for high performance amperometric glucose sensor. *Electroanalysis* **19**, 1008–1014 (2007).
- Fan, Z. Y., Wang, D. W., Chang, P. C., Tseng, W. Y. & Lu, J. G. ZnO nanowire field-effect transistor and oxygen sensing property. *Appl. Phys. Lett.* **85**, 5923–5925 (2004).
- Li, Q. H., Liang, Y. X., Wan, Q. & Wang, T. H. Oxygen sensing characteristics of individual ZnO nanowire transistors. *Appl. Phys. Lett.* **85**, 6389–6391 (2004).
- Wang, X. D., Song, J. H., Liu, J. & Wang, Z. L. Direct-current nanogenerator driven by ultrasonic waves. *Science* **316**, 102–105 (2007).
- Qin, Y., Wang, X. D. & Wang, Z. L. Microfibre–nanowire hybrid structure for energy scavenging. *Nature* **451**, 809–813 (2008).
- Liu, J., Fei, P., Zhou, J., Tummala, R. & Wang, Z. L. Toward high output-power nanogenerator. *Appl. Phys. Lett.* **92**, 173105 (2008).
- Xu, S., Wei, Y. G., Liu, J., Yang, R. & Wang, Z. L. Integrated multilayer nanogenerator fabricated using paired nanotip-to-nanowire brushes. *Nano Lett.* **8**, 4027–4032 (2008).
- Xu, S. *et al.* Optimizing and improving the growth quality of ZnO nanowire arrays guided by statistical design of experiments. *ACS Nano* **3**, 1803–1812 (2009).
- Lee, S. H. *et al.* Ordered arrays of ZnO nanorods grown on periodically polarity-inverted surfaces. *Nano Lett.* **8**, 2419–2422 (2008).
- Jasinski, J., Zhang, D., Parra, J., Katkanant, V. & Leppert, V. J. Application of channeling-enhanced electron energy-loss spectroscopy for polarity determination in ZnO nanopillars. *Appl. Phys. Lett.* **92**, 093104 (2008).
- Bae, S. Y. *et al.* Synthesis of gallium nitride nanowires with uniform [001] growth direction. *J. Cryst. Growth* **258**, 296–301 (2003).
- Liu, C. *et al.* Vapor–solid growth and characterization of aluminum nitride nanocones. *J. Am. Chem. Soc.* **127**, 1318–1322 (2005).
- Yang, R. S., Qin, Y., Dai, L. M. & Wang, Z. L. Power generation with laterally packaged piezoelectric fine wires. *Nature Nanotech.* **4**, 34–39 (2009).
- Wang, X. D., Liu, J., Song, J. H. & Wang, Z. L. Integrated nanogenerators in biofluid. *Nano Lett.* **7**, 2475–2479 (2007).
- Yang, R. S., Qin, Y., Li, C., Dai, L. M. & Wang, Z. L. Characteristics of output voltage and current of integrated nanogenerators. *Appl. Phys. Lett.* **94**, 022905 (2009).
- Shen, D. N. *et al.* Micromachined PZT cantilever based on SOI structure for low frequency vibration energy harvesting. *Sens. Actuat. A* **154**, 103–108 (2009).
- Roundy, S., Wright, P. K. & Rabaey, J. A study of low level vibrations as a power source for wireless sensor nodes. *Comput. Commun.* **26**, 1131–1144 (2003).
- Gao, Y. & Wang, Z. L. Electrostatic potential in a bent piezoelectric nanowire. The fundamental theory of nanogenerator and nanopiezotronics. *Nano Lett.* **7**, 2499–2505 (2007).
- Yang, R. S., Qin, Y., Li, C., Zhu, G. & Wang, Z. L. Converting biomechanical energy into electricity by a muscle-movement-driven nanogenerator. *Nano Lett.* **9**, 1201–1205 (2009).
- Choi, M. Y. *et al.* Mechanically powered transparent flexible charge-generating nanodevices with piezoelectric ZnO nanorods. *Adv. Mater.* **21**, 2185–2189 (2009).
- Qin, Y., Yang, R. S. & Wang, Z. L. Growth of horizontal ZnO nanowire arrays on any substrate. *J. Phys. Chem. C* **112**, 18734–18736 (2008).
- Song, J. H., Zhou, J. & Wang, Z. L. Piezoelectric and semiconducting coupled power generating process of a single ZnO belt/wire. A technology for harvesting electricity from the environment. *Nano Lett.* **6**, 1656–1662 (2006).
- Agrawal, R., Peng, B. & Espinosa, H. D. Experimental–computational investigation of ZnO nanowires strength and fracture. *Nano Lett.* **9**, 4177–4183 (2009).
- Kang, B. S. *et al.* pH measurements with single ZnO nanorods integrated with a microchannel. *Appl. Phys. Lett.* **86**, 112105 (2005).
- Zhou, J. *et al.* Gigantic enhancement in response and reset time of ZnO UV nanosensor by utilizing Schottky contact and surface functionalization. *Appl. Phys. Lett.* **94**, 191103 (2009).
- Li, Z. *et al.* Cellular level biocompatibility and biosafety of ZnO nanowires. *J. Phys. Chem. C* **112**, 20114–20117 (2008).
- Gao, Z. Y., Ding, Y., Lin, S. S., Hao, Y. & Wang, Z. L. Dynamic fatigue studies of ZnO nanowires by *in situ* transmission electron microscopy. *Phys. Status Solidi* **3**, 260–262 (2009).
- Xu, S., Lao, C. S., Weintraub, B. & Wang, Z. L. Density-controlled growth of aligned ZnO nanowire arrays by seedless chemical approach on smooth surfaces. *J. Mater. Res.* **23**, 2072–2077 (2008).
- Pan, Z. W., Dai, Z. R. & Wang, Z. L. Nanobelts of semiconducting oxides. *Science* **291**, 1947–1949 (2001).
- Zang, J. F. *et al.* Tailoring zinc oxide nanowires for high performance amperometric glucose sensor. *Electroanalysis* **19**, 1008–1014 (2007).

Acknowledgements

Research was supported by National Science Foundation (DMS 0706436, CMMI 0403671, ENG/CMMI 112024), the Defense Advanced Research Projects Agency (DARPA) (Army/AMCOM/REDSTONE AR, W31P4Q-08-1-0009) and the Department of Energy (Basic Energy Science) (DE-FG02-07ER46394), DARPA/ARO W911NF-08-1-0249. The authors would like to thank P. Fei, J. Zhou and T.-Y. Wei for technical assistance.

Author contributions

Z.L.W., S.X., Y.Q. and C.X. designed the experiments. S.X., Y.Q., C.X. Y.G.W. and R.S.Y. performed the experiments. Z.L.W., S.X., Y.Q. and C.X. analysed the data and wrote the paper. All authors discussed the results and commented on the manuscript.

Additional information

The authors declare no competing financial interests. Supplementary information accompanies this paper at www.nature.com/naturenanotechnology. Reprints and permission information is available online at <http://npg.nature.com/reprintsandpermissions/>. Correspondence and requests for materials should be addressed to Z.L.W.